

Observation of Long-Term Stable Response in MAPbBr₃ Single Crystals Monitored through Displacement Currents under Varying Illumination

Marisé García-Batlle,* Waqas Zia, Clara A. Aranda, Michael Saliba, Osbel Almora, Antonio Guerrero, and Germà Garcia-Belmonte*

Long life of perovskite devices in working conditions remains the bottleneck for technology application. Stable charge carriers' transport together with nonreactive contact materials contributes to the increase of the device operation time. Still, an appropriate model for transport carrier mechanisms is needed because of the complex ionic–electronic interplay. Herein, methylammonium lead bromide perovskite single crystals are used to analyze the current flowing across the perovskite sample after biasing. Two methods are performed: 1) direct measurement using an amperemeter and 2) indirect method by means of an induced potential in a reference capacitor. Because of the continuity of the current, the latest method measures direct current through the sample by monitoring displacements currents. Intriguing features are observed: the displacement currents result in stable and highly reproducible responses for long-term biasing (≈ 2000 s), while the direct measurements produce larger and exponentially increasing current dependence on time. These findings highlight the nontrivial effect of contacting and measuring procedures in exploring thick perovskite electrical response.

nonradiative carrier recombination rate, and facile fabrication.^[2] They have been successfully used in many optoelectronic applications, such as solar cells, lasers, light-emitting diodes (LEDs), or sensors.^[3] Recently, metal halide perovskite single crystals (SCs) have attracted great attention as high-efficiency photodetectors.^[4–7] Their unique combination of semiconducting properties and the large cross section for energetic photon as well as specific detectivity^[8] make them highly attractive candidates for X- and γ -rays detection.

However, long-term operation requires stable charge carrier transport properties to optimize charge collection and increase spatial resolution.^[9] Previous studies with perovskite SCs have reported that ions migrate under an external electric field causing the accumulation of mobile ionic species at the interfaces. This modulates

the net built-in electric field, changing the injection barriers for electronic carriers.^[10,11] The presence of moving ions modifies the current–voltage curves in perovskite solar cells, in addition to electronic mechanisms.^[12–14] In particular, slow redistribution of ions are responsible for the hysteretic behavior.^[15,16]

Because of the recognized influence of ion migration, several hypotheses have been suggested to distinguish ionic from electronic contributions to the measured current density flowing across the samples.^[11,17–21] Moreover, ionic transport has been investigated by different methods.^[9,18,22,23] Nevertheless, there is no conclusive evidence nor consensus on the most appropriate model when the analysis of direct current is addressed.^[24–26] Very recently, the use of a guard ring electrode configuration,^[27] which avoids recollection of crystal surface currents, has allowed to identify bulk transport up to 10 times lower than surface contributions.^[28] Those last findings may indicate a dependence of measured current on the contact configuration and registering method.

Here, we select perovskite SCs of methylammonium lead bromide (MAPbBr₃), which exhibit environmental stability,^[29,30] symmetrically contacted with Pt electrodes. By using this configuration, the effects of grain boundaries and internal interfaces can be discarded and, more importantly, the less reactive Pt metal is used,^[31,32] compared to Au, Ag, or even Cr, that reacts with the perovskite layer, reducing irreversible degradation.^[33] Pt contacts have been already employed for highly sensitive,


1. Introduction

Perovskite materials have exceptional properties such as high carrier mobility,^[1] long diffusion lengths, strong solar absorption, low

M. García-Batlle, O. Almora, A. Guerrero, G. Garcia-Belmonte
Institute of Advanced Materials (INAM)
Universitat Jaume I
12006 Castelló, Spain
E-mail: garciag@uji.es; batlle@uji.es

W. Zia, C. A. Aranda, M. Saliba
Institut für Photovoltaik (ipv)
University of Stuttgart
70569 Stuttgart, Germany

W. Zia, C. A. Aranda, M. Saliba
Helmholtz Young Investigator Group FRONTRUNNER
IEK5-Photovoltaik, Forschungszentrum Jülich
52425 Jülich, Germany

 The ORCID identification number(s) for the author(s) of this article can be found under <https://doi.org/10.1002/solr.202200173>.

© 2022 The Authors. Solar RRL published by Wiley-VCH GmbH. This is an open access article under the terms of the Creative Commons Attribution-NonCommercial-NoDerivs License, which permits use and distribution in any medium, provided the original work is properly cited, the use is non-commercial and no modifications or adaptations are made.

DOI: 10.1002/solr.202200173

long-term stable X-ray imaging systems.^[34] Due to the contacting symmetrical configuration, the perovskite layer is not subject to any electronic internal built-in potential that would otherwise afflict contact metals with different work functions.^[35]

The experimental procedure to study current mechanisms is based on transient charging signals. Our measurements record displacement currents i_{dis} in a reference capacitor C_0 , as sketched in **Figure 1a**, induced by the direct current i_{dir} flowing through the sample. This method monitors the voltage V_0 across C_0 such that the charge at the reference capacitor results as $Q = C_0 V_0$. Because the current continuity equation, $i_{dir} = i_{dis}$ at any time. This method is in contrast to the measurement of direct currents as depicted in **Figure 1b** using an amperemeter. Although it would be expected that both techniques monitor similar transport properties (electrical current through thick MAPbBr₃ SCs), significant differences are observed here between the time evolution and value of the current depending on the measuring method. While the use of the reference capacitor setup results in highly stable responses for long-term biasing (≈ 2000 s), the direct measurements produce larger and more featured current dependence on time. Our findings shed new light on the otherwise elusive analysis of electrical properties of perovskite materials, highlighting the nontrivial effect of contacting and measuring procedures.

2. Results and Discussion

In **Figure S1**, Supporting Information, we show the general electrical behavior of a single-crystal perovskite sample of

MAPbBr₃. The ohmic character (slope ≈ 1) observed in the i - V curve is remarkable and agrees with some previous studies of symmetrical SCs perovskite-based devices,^[9,11,36,37] but not necessarily true for longer times.^[10] Note that the typical measuring time of the i - V curve situates at ≈ 100 s. **Figure 1a** shows the configuration of the setup circuit for the measurement of charge at the reference capacitor. Here, a step voltage pulse (V_{app}) is applied to the sample Z_x (which is modeled by a parallel combination of C_x and R_x) across a linear reference capacitor C_0 , with both elements in series connection. Here, C_x and R_x account for the low-frequency capacitance and shunt resistance of the sample, respectively. The analysis is meaningful if the applied voltage principally drops within the perovskite sample, i.e., $V_0 \ll V_{app}$. This is accomplished when $C_0 \gg C_x$ and the measuring time is restricted to $t \ll R_x C_0$ (see transfer function in Section S2, Supporting Information). Thereupon, the charge storage in C_0 is $Q = C_0 V_0$, being V_0 the voltage at the reference capacitor (see **Figure 1b**), which is recorded through an ultrahigh input resistance unity gain field-effect-transistor buffer with 10 T Ω to avoid loading effects from the recording instrument. As observed in **Figure 1b**, the voltage at C_0 follows the bias perturbation steps by just a small amount. It is worth noting that the displacement current in the reference capacitor equals the current flowing in the sample for $t \gg R_x C_x$. Hence, a simple calculation (see Section S2, Supporting Information) allows to derive the induced charge Q in C_0 as $Q(t) = V_{app}(1 - e^{-t/R_x C_0})/R_x$ that for shorter times

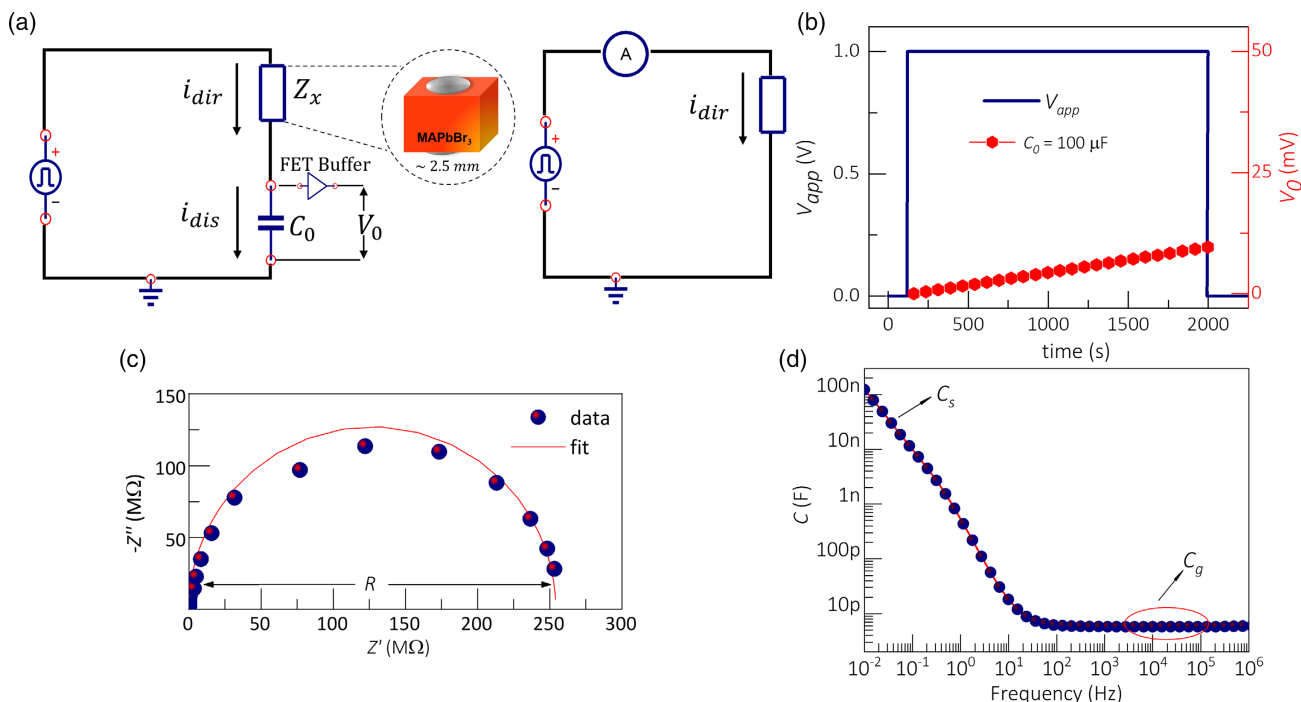


Figure 1. a) Experimental setup used to record charge transient measurements (left) and direct electronic currents (right) of 2 mm-thick MAPbBr₃ SC. b) Charge transient response in the dark conditions. The applied rectangular pulse (V_{app}) of 1 V height is compared with the induced voltage V_0 (note the scale differences). c) Impedance and d) capacitance spectra of 2 mm-thick MAPbBr₃ SC, measured at 0 V bias in dark. **Figure S10**, Supporting Information, shows the equivalent circuit used to fit the impedance spectra.

simply results in $Q(t) = V_{\text{app}}t/R_x$. In other words, our procedure allows indirectly to measure the current through the sample as $i = V_{\text{app}}/R_x$ that is simply integrated in C_0 .

An estimation of the elements R_x and C_x can be derived from the impedance and capacitance spectra, registered at zero bias of MAPbBr₃ SCs as shown in Figure 1c,d. The trends exhibited agree with prior measurements in SCs reported in the literature.^[10,11] From the impedance spectra (Figure 1c), one can observe at high and intermediate frequencies ($f > 100$ Hz) the sample shunt resistance R and the geometrical capacitance $C_g \approx 6.3$ pF to dominate the response. In the Nyquist plot this can be identified as a semicircle through the RC_g coupling. However, a low-frequency feature is observed by analyzing the capacitance response, which is commonly known as excess capacitance C_s .^[38,39] This excess capacitance $C_s \gg C_g$ accounts for the increase in charge density near the interfaces, and it exceeds by several orders of magnitude that is occurring in the bulk. In the dark, this low-frequency capacitance exhibits a thickness-independent trend and has been related to ionic polarization/dynamics within the material.^[38–40] Note, however, that the actual R_x and C_x may slightly differ from the values $C_s \approx 100$ nF and $R \approx 250$ M Ω because of the dissimilar explored time window. In any case, the time constant $R_x C_x \approx 100$ s results much shorter than the measuring times used here.

Figure 2a shows the charge transient signals obtained in the dark using the setup in Figure 1a and reference capacitors within the range of $C_0 = 1\text{--}470$ μF , which were previously checked using impedance analysis (see Figure S6, Supporting Information). For the reference capacitors spectra, one can observe a plateau at the frequencies ($f < 1$ kHz) which is the region of interest. By analyzing the voltage response in Figure S5, Supporting Information, upon application of 1 V bias step, it is inferred that V_0 inversely scales with the reference capacitor, as expected. The condition $V_0 \ll V_{\text{app}}$ is accomplished in this case when V_0 attains values $\ll 1$ V. By examining Figure S7a, Supporting Information, the polarization charge $Q = C_0 V_0$ results independent on the reference capacitor when $C_0 > 10$ μF . Lower capacitance values do not assure that the applied voltage principally drops within the perovskite sample because the condition $t \ll R_x C_0$ is no longer accomplished. Therefore, when using larger values of C_0 all response curves collapse in most of the transient for the explored time windows (up to 2000 s). From the estimations of the long-term accumulated charge Q_{LT} , in Figure S7b, Supporting Information, one can see that it attains values within the range of ≈ 1100 nC (after ≈ 2000 s). Note that lower charge values are encountered for smaller values of C_0 as expected. It is then concluded here that the charge induced in the reference capacitor stems from the perovskite shunt resistance upon long-term (≈ 2000 s) biasing, as demonstrated by the collapse of the transient charge signals as far as $C_0 > 10$ μF . High reproducibility is also noticed despite long-term biasing periods. Recalling now the impedance spectra in Figure 1d, a geometrical capacitance $C_g \approx 5$ pF and a bias $V_{\text{app}} = 1$ V in dark condition imply a charge $Q_b = C_g V_{\text{app}}$ approximately equal to 5 pC, which does not match those encountered from Figure S7, Supporting Information. Such a huge value ($Q \approx 1100$ nC) cannot be linked then to the polarization of the perovskite bulk.

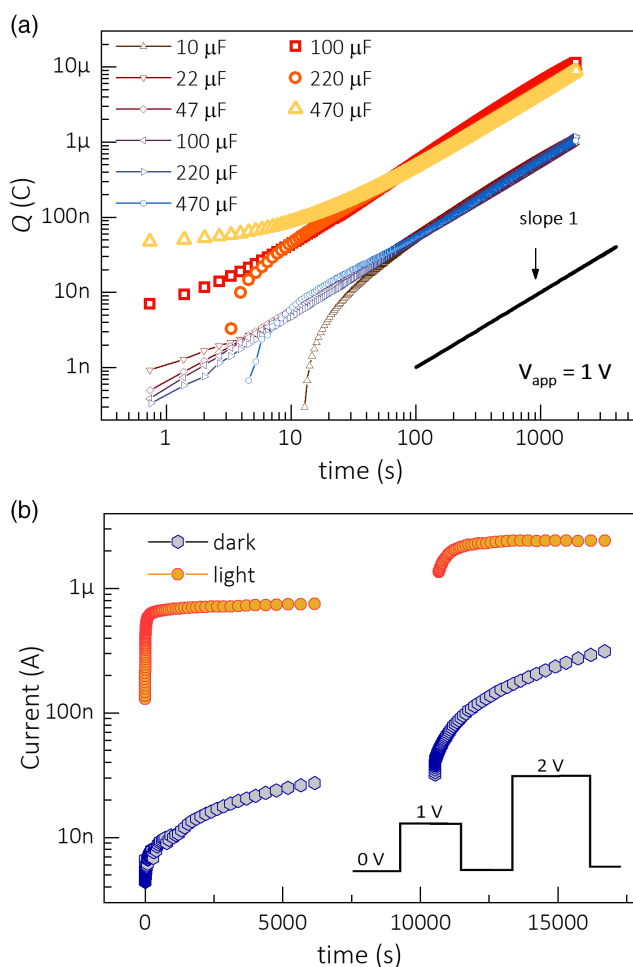


Figure 2. a) Comparison between the charge transient responses in the dark and light conditions (100 mW cm^{-2}) under 1 V applied bias. The solid black line corresponds to slope 1. b) Electronic current transient response in the dark and light conditions upon two different biases for a ≈ 2.5 mm-thick MAPbBr₃ SCs sample. Noted that the electronic current exponentially rises until steady-state values upon the biasing protocol (in the inset) at long times.

Now let us analyze the charge transient signal under an irradiance intensity of 100 mW cm^{-2} (see Figure S8, Supporting Information). As inferred from our previous results in dark condition, the use of a large enough reference capacitor ensures that the voltage mainly drops at the perovskite SCs. Under illumination, only values of $C_0 > 100$ μF can be used to obtain meaningful transient measurements (collapse of the charge transient into a single response) as observed in Figure 2a. By comparing the charging transient response, both in dark and light in Figure 2a, one can infer a good linear relationship between Q and t for the time window explored. By fitting, it is parameterized as $Q(t) = it$ as previously derived with slope 1. Therefore, a value for the constant charging current i results in (0.51 ± 0.06) nA in the dark and (4.87 ± 0.03) nA under continuous light irradiation. It is inferred then that light enhances current through the perovskite sample by reducing the shunt resistance (photoresistive effect) by approximately one order of magnitude. More

importantly, one can state that both dark and light currents exhibit an extremely stable and reproducible response, in contrast to that obtained through direct current analysis as next explained.

To elucidate the origin of those currents measured by dielectric displacement at C_0 , we explore electronic currents plotted in Figure 2b, in which the long-term current response upon the direct application of voltage steps to the sample in dark conditions is shown. The general protocol of measurement in Figure 2b is based on previous reports^[10]: first the crystals are polarized for 3 h and then left to relax at 0 V for 2 h. As recently reported, direct currents originate from a drift of electronic species kinetically controlled by migrating ions.^[10] However, a significant difference appears in comparison to the charging method: currents are no longer constant but increase with time. For times of ≈ 2000 s and 1 V bias, electronic dark current achieves values approximately equal to 10 nA, much greater than that registered through C_0 . If charge transients are programmed for even longer time (see Figure S9, Supporting Information), the same linear relationship is still observed. Under illumination, the differences are even larger: direct measurement attains ≈ 800 nA, while the reference capacitor setup yields only ≈ 5 nA. The measurement of induced potentials registers displacement currents in C_0 and, indirectly, constant current across shunt resistor. Our findings point out the significant influence of the method employed for charge extraction at the contacts that enlarge recombination currents. This is suggested by the drastic reduction in measured current under illumination when the reference capacitor setup is used in comparison with the direct one. While long-term flowing current is reduced by a factor of 20 with the capacitor setup in dark, under illumination that suppression attains even larger values ($i_{\text{dir}}/i_{\text{dis}} \approx 160$). Those comparisons move us to conjecture about the different charging nature of the contacts. In one case (direct current measurement), low contact is directly grounded what assures sufficient and rapid removing of interfacial charges by the measuring setup. On the contrary, with the reference capacitor method arriving charges should remain at the contacts (to maintain the measured voltage) which promotes the occurrence of additional mechanism such as enhancement of surface recombination currents. Although our findings are certainly very preliminary and a more systematic analysis is needed, they seem to point out the determining role of the charging at the contacts (interfacial carrier density) to establish the steady-state current flow. We can even propose a change in the current-governing process: capacitor setup effectively registers minimum bulk conduction currents resulting after large surface carrier recombination, while direct measurement does not activate such as interfacial mechanisms and produces, as a consequence, larger currents are measured.

3. Conclusion

A fundamental difference is reported here when flowing currents are registered either directly or indirectly using an induced potential. The use of the reference capacitor setup suppresses direct current by monitoring exclusively displacements currents in C_0 . This is corroborated by the collapse of the charge transients, in which the polarization voltages stem from current flowing

through the shunt resistance. Under illumination, excess electronic carriers are generated, which enlarge currents by a photoresistive effect. Our findings alert us on the variability in the measured electrical current across the sample depending on the experimental method, which may be used to guide us in the pursuit of a robust electrical model that accounts for contact mechanisms (at the end responsible of the measured electrical characteristics in perovskite-based devices) in addition to bulk conduction. A better understanding of the charging mechanisms at the contacts and how the surface carrier kinetics intervene in establishing the steady-state current allows us to progress into the halide perovskite device physics and operating modes.

4. Experimental Section

Solution Growth: All materials used for the preparation of the SCs were used as received: $\text{CH}_3\text{NH}_3\text{Br}$ (> 99 wt%) and PbBr_2 (99.999 wt%) were purchased from Dyesol and TCI America, respectively; dimethylformamide (DMF) (anhydrous, 99.8 wt%) was purchased from Sigma-Aldrich. Salts were stored in a glove box under N_2 atmosphere. Among the different methods for the growth of MAPbBr_3 SCs, the inverse temperature crystallization (ITC) in DMF was used through which the obtained SCs exhibit a cubic shape (see Figure S1, Supporting Information, inset) that makes them suited for the fabrication of devices. For the growth experiments, the perovskite precursors, $\text{CH}_3\text{NH}_3\text{Br}$ and PbBr_2 , were dissolved (1:1 mol%) in DMF to obtain 1 M solutions of MAPbBr_3 . All the solutions were first maintained at room temperature under stirring and then filtered using PTFE filters with 0.2 μm pore size to remove any insoluble particles. Two growth protocols were investigated labeled as fast/unseeded and slow/seeded growth. The process was similar to the one described in a previous work^[36] using a linear temperature ramp. Seeds must be first obtained by spontaneous nucleation and used subsequently for crystal growth; the quality of the seed depends on the geometry of the vials and the temperature profile. For the fast/unseeded protocol, derived from the ITC method,^[36,41] 3 mL of perovskite solutions is placed in 20 mL glass flask vial, using a silicon oil bath; the temperature is abruptly brought from room to 80–85 °C leading to the spontaneous nucleation and growth of crystals. In the slow/seeded procedure, the heating temperature profile is crucial. With the same perovskite solution, the temperature is first increased at 50 °C, and then is kept for 20 min at this temperature to place the seeds inside the flasks to avoid dissolving the seed. Finally, the solution is heated up, at a constant heating rate of 10 °C h^{-1} for 3 h, until 80–85 °C. The crystals obtained are washed with warm DMF, then placed in the vial, and transferred to the dry box with a nitrogen atmosphere. In the end, SCs were mechanically polished with three different sandpaper—P1200 (15 μm), P2400 (10 μm), and P4000 (5 μm)—and Pt electrodes were sputtered at two opposite faces.

Device Preparation and Optical Characterization: Interface-mediated mechanisms are recognized to constitute issues of primary concern at the perovskite/metal electrode interface.^[42] It has been reported that Platinum is a preferably significantly inert material which does not react with the perovskite films.^[43,44] Then, Pt was sputtered (≈ 30 nm) at opposite sides of the SCs and Au was thermally evaporated (100 nm) on top of Pt, at 6×10^{-6} mbar, to protect the metallic contact. The SCs were characterized by UV–vis absorption spectra in Cary 500 Scan VARIAN spectrophotometer (250–900 nm), obtaining the distinctive spectra with the corresponding absorption edge at for MAPbBr_3 with a bandgap of 2.18 eV (see Tauc plot, inset Figure S2, Supporting Information). The photoluminescence measurements were collected by a Fluorolog3-11 Horiba, using a 405 nm excitation source; the photoluminescence peak position (≈ 570 nm) of MAPbBr_3 is observed in Figure S2, Supporting Information, and matches the values reported earlier for the same SCs.^[41,45] Also, Figure S3, Supporting Information, shows the XRD patterns of MAPbBr_3 obtained with a D8 Endeavor diffractometer equipped with a Johansson monochromator. The SCs were grinded into powder

and measured in Bragg–Brentano θ – 2θ geometry. The diffractogram reveals the standard cubic space group Pm3m of MAPbBr₃ crystals with lattice dimension $a = 5.928 \text{ \AA}$ and without any trace of the secondary phase. Using an X-Ray diffractometer Agilent Super Nova Atlas Dual Source (Cu K α , wavelength $\lambda = 1.5406 \text{ \AA}$), an XRD-2D rotation spectrum along the α cell axis was measured. In Figure S4, Supporting Information, only dots appear; the absence of concentrically distributed circles is a clear sign that the material is not polycrystalline.^[46] For the light condition measurements, a Si photodiode was used to calibrate the system and transient curves were performed under 1 sun illumination (100 mW cm^{-2}) using an OSL2-High-Intensity Fiber-Coupled Illuminator (Thorlabs).

Electrical Measurements: All electrical experiments were performed at room temperature in the air. Direct impedance measurements were carried out by using a PGSTAT-30 Autolab potentiostat equipped with impedance module. Samples were measured inside a shielded cryostat Alpha dielectric E4991A Novocontrol acting as Faraday cage, in dark conditions between 10 mHz and 1 MHz, with a perturbation amplitude of 1 V. For the charging measurements using a reference capacitor, a source measure unit Keithley Model 2612 was used as the voltage supply and the polarization voltage signals, shown in Figure S5, Supporting Information, were recorded with a HP Digital Multimeter Model 34401A (input impedance $> 10 \text{ G}\Omega$) coupled through a FET input buffer model AD8244 (input impedance $10 \text{ T}\Omega$). The thicknesses of the samples are around $\approx 2.5 \text{ mm}$, and the evaporated electrodes had an active area of $\approx 13 \text{ mm}^2$. A Broadband Halogen Fiber Optic lamp (150 W high output) with an irradiance level of 100 mW cm^{-2} was used.

Supporting Information

Supporting Information is available from the Wiley Online Library or from the author.

Acknowledgements

This work has received funding from the European Union's Horizon 2020 research and innovation program under the Photonics Public Private Partnership with the project PEROXIS under Grant Agreement No. 871336. G.G.-B. acknowledges the financial support from Ministerio de Ciencia e Innovación (Spain) under project no. PID2019-107348GB-I00. M.G.-B. acknowledges the support for the research stay from Generalitat Valenciana (BEFPI2020) under the grant number (GRISOLIAP/2018/073). The authors also acknowledge SCIC from UJI for Pt deposition. M.S. thanks the German Research Foundation (DFG) for funding (SPP2196, 431314977/GRK 2642). M.S. acknowledges funding by ProperPhotoMile. Project ProperPhotoMile is supported under the umbrella of SOLAR-ERA.NET Cofund 2 by The Spanish Ministry of Science and Education and the AEI under the project PCI2020-112185 and CDTI project number IDI-20210171; the Federal Ministry for Economic Affairs and Energy on the basis of a decision by the German Bundestag project number FKZ 03EE1070B and FKZ 03EE1070A and the Israel Ministry of Energy with project number 220-11-031. SOLAR-ERA.NET is supported by the European Commission within the EU Framework Programme for Research and Innovation HORIZON 2020 (Cofund ERA-NET Action, No. 786483). C.A.A. thanks the Helmholtz Young Investigator Group FRONTRUNNER.

Funding for open access charge: CRUE-Universitat Jaume I. The funding information was updated on September 9, 2022.

Conflict of Interest

The authors declare no conflict of interest.

Data Availability Statement

The data that support the findings of this study are available from the corresponding author upon reasonable request.

Keywords

direct current, halide perovskites, impedance spectroscopy, transient experiments

Received: February 23, 2022

Revised: June 4, 2022

Published online: July 10, 2022

- [1] M. A. Green, A. Ho-Baillie, H. J. Snaith, *Nat. Photonics* **2014**, *8*, 506.
- [2] N. Onoda-Yamamuro, T. Matsuo, H. Suga, *J. Phys. Chem. Solids* **1992**, *53*, 935.
- [3] M. H. Futscher, M. K. Gangishetty, D. N. Congreve, B. Ehrler, *J. Chem. Phys.* **2020**, *152*, 044202.
- [4] M. A. Afroz, C. A. Aranda, N. K. Mar Tailor, Yukta, P. Yadav, M. M. Tavakoli, M. Saliba, S. Satapathi, *ACS Energy Lett.* **2021**, *6*, 3275.
- [5] Y. He, M. Petryk, Z. Liu, D. G. Chica, I. Hadar, C. Leak, W. Ke, I. Spanopoulos, W. Lin, D. Y. Chung, B. W. Wessels, Z. He, M. G. Kanatzidis, *Nat. Photonics* **2021**, *15*, 36.
- [6] Y. Liu, Z. Yang, S. Liu, *Adv. Sci.* **2018**, *5*, 1700471.
- [7] H. Wei, Y. Fang, P. Mulligan, W. Chuirazzi, H. H. Fang, C. Wang, B. R. Ecker, Y. Gao, M. A. Loi, L. Cao, J. Huang, *Nat. Photonics* **2016**, *10*, 333.
- [8] Y. Liu, Y. Zhang, K. Zhao, Z. Yang, J. Feng, X. Zhang, K. Wang, L. Meng, H. Ye, M. Liu, S. Liu, *Adv. Mater.* **2018**, *30*, 1707314.
- [9] O. Baussens, L. Maturana, S. Amari, J. Zaccaro, J.-M. Verilhac, L. Hirsch, E. Gros-Daillon, *Appl. Phys. Lett.* **2020**, *117*, 041904.
- [10] M. García-Battle, J. M. Guillén, M. Chapran, O. Baussens, J. Zaccaro, E. Gros Daillon, J. M. Verilhac, A. Guerrero, O. Almora, G. Garcia Belmonte, *ACS Energy Lett.* **2022**, *7*, 946.
- [11] M. García-Battle, O. Baussens, S. Amari, J. Zaccaro, E. Gros-Daillon, J. M. Verilhac, A. Guerrero, G. Garcia-Belmonte, *Adv. Electron. Mater.* **2020**, *6*, 2000485.
- [12] W. Tress, N. Marinova, T. Moehl, S. M. Zakeeruddin, M. K. Nazeeruddin, M. Grätzel, *Energy Environ. Sci.* **2015**, *8*, 995.
- [13] R. Gottesman, E. Haltzi, L. Gouda, S. Tirosh, Y. Bouhadana, A. Zaban, E. Mosconi, F. De Angelis, *J. Phys. Chem. Lett.* **2014**, *5*, 2662.
- [14] F. Ebadi, N. Taghavinia, R. Mohammadpour, A. Hagfeldt, W. Tress, *Nat. Commun.* **2019**, *10*, 1574.
- [15] J. M. Azipiroz, E. Mosconi, J. Bisquert, F. De Angelis, *Energy Environ. Sci.* **2015**, *8*, 2118.
- [16] C. Eames, J. M. Frost, P. R. F. Barnes, B. C. O'Regan, A. Walsh, M. Saiful Islam, *Nat. Commun.* **2015**, *6*, 7497.
- [17] M. García-Battle, S. Deumel, J. E. Huedler, S. F. Tedde, A. Guerrero, O. Almora, G. Garcia-Belmonte, *ACS Appl. Mater. Interfaces* **2021**, *13*, 35617.
- [18] W. Peng, C. Aranda, O. M. Bakr, G. Garcia-Belmonte, J. Bisquert, A. Guerrero, *ACS Energy Lett.* **2018**, *3*, 1477.
- [19] D. Wei, F. Ma, R. Wang, S. Dou, P. Cui, H. Huang, J. Ji, E. Jia, X. Jia, S. Sajid, A. M. Elseman, L. Chu, Y. Li, B. Jiang, J. Qiao, Y. Yuan, M. Li, *Adv. Mater.* **2018**, *30*, 1707583.
- [20] E. L. Unger, E. T. Hoke, C. D. Bailie, W. H. Nguyen, A. R. Bowring, T. Heumüller, M. G. Christoforo, M. D. McGehee, *Energy Environ. Sci.* **2014**, *7*, 3690.
- [21] Z. Xiao, Y. Yuan, Y. Shao, Q. Wang, Q. Dong, C. Bi, P. Sharma, A. Gruverman, J. Huang, *Nat. Mater.* **2015**, *14*, 193.
- [22] M. A. Afroz, C. A. Aranda, N. K. Tailor, X. Yukta, P. Yadav, M. M. Tavakoli, M. Saliba, S. Satapathi, *ACS Energy Letters* **2021**, *6*, 3275.

- [23] A. Musienko, J. Pipek, P. Praus, M. Brynza, E. Belas, B. Dryzhakov, M.-H. Du, M. Ahmadi, R. Grill, *Sci. Adv.* **2020**, *6*, eabb6393.
- [24] M. H. Futscher, J. V. Milić, *Front. Energy Res.* **2021**, *9*, 629074.
- [25] H. Wang, A. Guerrero, A. Bou, A. M. Al-Mayouf, J. Bisquert, *Energy Environ. Sci.* **2019**, *12*, 2054.
- [26] E. A. Duijnste, V. M. Le Corre, M. B. Johnston, L. J. Anton Koster, J. Lim, H. J. Snaith, *Phys. Rev. Appl.* **2021**, *15*, 014006.
- [27] H. Wei, D. DeSantis, W. Wei, Y. Deng, D. Guo, T. J. Savenije, L. Cao, J. Huang, *Nat. Mater.* **2017**, *16*, 826.
- [28] O. Almora, G. J. Matt, A. These, A. Kanak, I. Levchuk, S. Shrestha, A. Osvet, C. J. Brabec, G. Garcia-Belmonte, *J. Phys. Chem. Lett.* **2022**, *13*, 3824.
- [29] J. I. J. Choi, M. E. Khan, Z. Hawash, K. J. Kim, H. Lee, L. K. Ono, Y. Qi, Y.-H. Kim, J. Y. Park, *J. Mater. Chem. A* **2019**, *7*, 20760.
- [30] C. Wang, B. R. Ecker, H. Wei, J. Huang, Y. Gao, *J. Phys. Chem. C* **2018**, *122*, 3513.
- [31] A. Fakhruddin, L. Schmidt-Mende, G. Garcia-Belmonte, R. Jose, I. Mora-Sero, *Adv. Energy Mater.* **2017**, *7*, 1700623.
- [32] A. Guerrero, J. You, C. Aranda, Y. S. Kang, G. Garcia-Belmonte, H. Zhou, J. Bisquert, Y. Yang, *ACS Nano* **2016**, *10*, 218.
- [33] B. Roose, Q. Wang, A. Abate, *Adv. Energy Mater.* **2019**, *9*, 1803140.
- [34] S. Deumel, A. van Breemen, G. Gelinck, B. Peeters, J. Maas, R. Verbeek, S. Shanmugam, H. Akkerman, E. Meulenkamp, J. E. Huerdler, M. Acharya, M. Garcia-Battle, O. Almora, A. Guerrero, G. Garcia-Belmonte, W. Heiss, O. Schmidt, S. F. Tedde, *Nat. Electron.* **2021**, *4*, 681.
- [35] Y. He, L. Matei, H. J. Jung, K. M. McCall, M. Chen, C. C. Stoumpos, Z. Liu, J. A. Peters, D. Y. Chung, B. W. Wessels, M. R. Wasielewski, V. P. Dravid, A. Burger, M. G. Kanatzidis, *Nat. Commun.* **2018**, *9*, 1609.
- [36] S. Amari, J.-M. Verilhac, E. G. D'Aillon, A. Ibanez, J. Zaccaro, *Cryst. Growth Des.* **2020**, *20*, 1665.
- [37] J. T. Tisdale, E. Muckley, M. Ahmadi, T. Smith, C. Seal, E. Lukosi, I. N. Ivanov, B. Hu, *Adv. Mater. Interfaces* **2018**, *5*, 1800476.
- [38] O. Almora, A. Guerrero, G. Garcia-Belmonte, *Appl. Phys. Lett.* **2016**, *108*, 043903.
- [39] O. Almora, I. Zarazua, E. Mas-Marza, I. Mora-Sero, J. Bisquert, G. Garcia-Belmonte, *J. Phys. Chem. Lett.* **2015**, *6*, 1645.
- [40] J. Caram, M. Garcia-Battle, O. Almora, R. D. Arce, A. Guerrero, G. Garcia-Belmonte, *Appl. Phys. Lett.* **2020**, *116*, 183503.
- [41] M. I. Saidaminov, A. L. Abdelhady, B. Murali, E. Alarousu, V. M. Burlakov, W. Peng, I. Dursun, L. Wang, Y. He, G. Maculan, A. Goriely, T. Wu, O. F. Mohammed, O. M. Bakr, *Nat. Commun.* **2015**, *6*, 7586.
- [42] L. Zhao, R. A. Kerner, Z. Xiao, Y. L. Lin, K. M. Lee, J. Schwartz, B. P. Rand, *ACS Energy Lett.* **2016**, *1*, 595.
- [43] P. A. Shaikh, D. Shi, J. R. D. Retamal, A. D. Sheikh, M. A. Haque, *J. Mater. Chem. C* **2016**, *4*, 8304.
- [44] M. Stumpp, R. Ruess, J. Müßener, D. Schlettwein, *Mater. Today Chem.* **2017**, *4*, 97.
- [45] D. Shi, V. Adinolfi, R. Comin, M. Yuan, E. Alarousu, A. Buin, Y. Chen, S. Hoogland, A. Rothenberger, K. Katsiev, Y. Losovyj, X. Zhang, P. A. Dowben, O. F. Mohammed, E. H. Sargent, O. M. Bakr, *Science* **2015**, *347*, 519.
- [46] N. Widjonarko, *Coatings* **2016**, *6*, 54.